ICONE12-49579

MATERIALS INTERACTION TESTS TO IDENTIFY BASE AND COATING MATERIALS FOR AN ENHANCED IN-VESSEL CORE CATCHER DESIGN

*J. L. Rempe, D. L. Knudson, K. G. Condie, and W. D. Swank
Idaho National Engineering and Environmental Laboratory
P. O. Box 1625
Idaho Falls, ID, USA, 83415-3840
*(P) 208-526-2897, (F) 208-526-2930, (E) yoj@inel.gov

K. Y. Suh
Seoul National University
Department of Nuclear Engineering
Seoul, Korea

F.-B. Cheung
The Pennsylvania State University
Department of Mechanical and Nuclear Engineering
University Park, PA, USA 16802

S.-B.Kim
Korea Atomic Energy Research Institute
Severe Accident Research Project
Taejon, Korea 305-600

ABSTRACT

An enhanced in-vessel core catcher is being designed and evaluated as part of a joint United States (U.S.) - Korean International Nuclear Engineering Research Initiative (INERI) investigating methods to insure In-Vessel Retention (IVR) of core materials that may relocate under severe accident conditions in advanced reactors. To reduce cost and simplify manufacture and installation, this new core catcher design consists of several interlocking sections that are machined to fit together when inserted into the lower head. If needed, the core catcher can be manufactured with holes to accommodate lower head penetrations. Each section of the core catcher consists of two material layers with an option to add a third layer (if deemed necessary): a base material, which has the capability to support and contain the mass of core materials that may relocate during a severe accident; an insulating oxide coating material on top of the base material, which resists interactions with high-temperature core materials; and an optional coating on the bottom side of the base material to prevent any potential oxidation of the base material during the lifetime of the reactor.

Initial evaluations suggest that a thermally-sprayed oxide material is the most promising candidate insulator coating for a core catcher. As part of the effort to develop an in-vessel core catcher design, a series of high temperature materials interaction tests were conducted for thermal sprayed coatings and base materials with properties deemed most promising. This paper reports results from these materials interactions tests and efforts to optimize parameters for applying the thermal spray coatings.

INTRODUCTION

If there were inadequate cooling during a reactor accident, a significant amount of core material could become molten and relocate to the lower head of the reactor vessel, as happened in the Three Mile Island Unit 2 (TMI-2) accident. If it is possible to ensure that the vessel head remains intact so that relocated core materials are retained within the vessel, the enhanced safety associated with these plants can reduce concerns about containment failure and associated risk. For example, the enhanced safety of the Westinghouse Advanced 600 MWe PWR (AP600), which relied upon External Reactor Vessel Cooling (ERVC) for In-vessel Retention (IVR), resulted in the U.S. Nuclear Regulatory Commission (US NRC) approving the design without requiring certain conventional features common to existing LWRs. Consequently, IVR of core melt is a key severe accident management strategy adopted by some operating nuclear power plants and proposed for some

Copyright © 2004 by ASME

advanced light water reactors (ALWRs). However, it is not clear that currently proposed ERVC, without additional enhancements, could provide sufficient heat removal for higher-power reactors (up to 1500 MWe).

Objective

A U.S. - Korean INERI project has been initiated in which the Idaho National Engineering and Environmental Laboratory (INEEL), Seoul National University (SNU), Pennsylvania State University (PSU), and the Korea Atomic Energy Research Institute (KAERI) will investigate the performance of ERVC and core catchers to determine if IVR is feasible for reactors up to 1500 MWe. This program is initially focusing on the Korean Advanced Power Reactor 1400 MWe (APR1400) design. However, improved margins relative to IVR offered by each modification will be evaluated such that methods can easily be applied to a wide range of existing and advanced reactor designs.

A major effort in this collaborative, three-year, INERI project is to develop an in-vessel core catcher design for the APR1400 and to provide sufficient data to demonstrate that this core catcher design will enhance in-vessel debris coolability. This paper describes high temperature tests that were conducted to determine if materials interactions occur at temperatures lower than the melting temperature of core catcher base and coating materials. In addition, results from sensitivity studies conducted to optimize thermal spray parameters for coating materials are reported.

Design Approach

The approach adopted for developing an APR1400 core catcher design is illustrated in Figure 1. As shown in this figure, initial efforts focused on developing a preliminary in-vessel design. This design relies on several mechanisms to enhance IVR, such as retention and dilution of the decay heat in the relocated core materials and heat transfer through the lower surface of the core catcher via narrow gap cooling.

As shown in the figure, the preliminary design was developed using a combination of scoping materials analyses, scoping flow analyses, scoping thermal analyses, scoping structural analyses, and scoping materials interaction tests. To demonstrate the viability of this design, more detailed calculations will be performed using SCDAP/RELAP5-3D$^©$ (INEEL, 2002) and results will be evaluated to assure that the core catcher can withstand estimated loads from relocated materials. In addition, more detailed data will be obtained in two areas. First, data are needed to estimate the heat that can be removed from the narrow "engineered" gap between the in-vessel core catcher and the inner surface of the reactor vessel lower head. As indicated in Figure 1, data

are being obtained from the Gap-cooling Apparatus against Molten Material Attack (GAMMA) facilities at SNU and the Critical Heat Flux in Gap (CHFG) facility at KAERI to formulate a complete "narrow gap" boiling curve. Second, data are needed to understand the heat loads to the core catcher and demonstrate the viability of materials proposed for the in-vessel core catcher. As illustrated in the figure, these needs will be addressed by conducting tests in several facilities: the Simulation of Internal Gravity-driven Melt Accumulation (SIGMA) facilities at SNU will be used to develop natural convection heat transfer correlations, the Lower-plenum Arrested Vessel Attack - Gap (LAVA-GAP) facility at KAERI will be used to assess heat loads from relocating material, and INEEL's high temperature prototypic test facility will be used to assess the potential for materials interactions.

Detailed information about the design and capabilities of these experimental facilities can be found in several references (e.g., Rempe, et al., 2002). The remainder of this paper is devoted to describing results from core catcher development efforts completed during the second year of this project. However, it should be noted that the core catcher design process is iterative. As data are obtained from various experimental facilities, it is anticipated that the preliminary core catcher design may be modified. Likewise, experimental test plans are impacted by results from other activities.
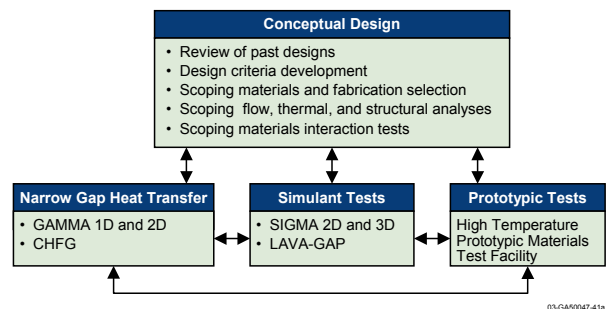
Figure 1. Activities to develop a core catcher.

BACKGROUND

Preliminary Core Catcher Design

A preliminary design was developed that builds upon an in-vessel core catcher concept proposed by Hwang and Suh (2001). However, the new core catcher design consists of several interlocking sections (see Figure 2). The use of multiple sections reduces cost, and simplifies manufacture and installation. The sections are machined such that they fit together when inserted into the lower head. For reactor designs with penetrations, such as the APR1400, the core catcher is manufactured with holes to accommodate lower head penetrations. Each section of

2   Copyright © 2004 by ASME

the core catcher (see Figure 2) consists of two material layers with an option to add a third layer (if deemed necessary): a base material, which has the capability to support and contain the mass of core materials that may relocate during a severe accident; an oxide coating material on top of the base material, which resists interactions with high-temperature core materials; and an optional coating on the bottom side of the base material to prevent any potential oxidation of the base material during the lifetime of the reactor.
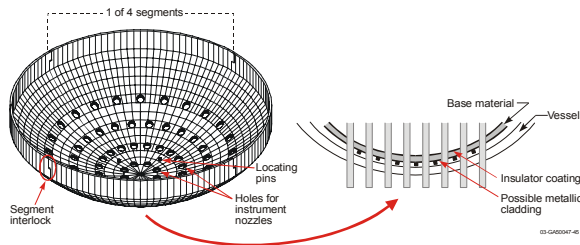
Figure 2. APR1400 core catcher conceptual design.

Various types of application methods, such as chemical vapor deposition, thermal plasma spraying, and painting, were reviewed; and preliminary evaluation suggests that the insulator coating should be applied via a plasma spray process. The plasma spray process, which is relatively inexpensive, can provide a chemically stable, rugged, dense, and bonded coating of materials for any desired thickness.

Thermal Plasma Spray Processes

Thermal spray processes originated with the concept known as flame spraying. A wide range of materials can be sprayed using a spray gun that performs the essential functions of heating and projecting the coating material through the use of an oxy-fuel flame and a pressurized carrier gas jet. The gun serves to atomize and melt or soften the material as it is fed into the flame, then ejects the soft or molten particles in a directed stream through the gun's nozzle. Variations in gun design allow either wire or powder to be used as the coating material feedstock and permit larger or smaller spray streams to be applied, as desired. Cooling and solidification of the sprayed material occurs upon contact with the substrate. The relatively low particle velocity of the flame spray process produces a thermal barrier coating of moderate density. Because the substrate is at a relatively low temperature, there is less concern about cracking of ceramic coatings as a result of differential thermal expansion upon cooling from an elevated temperature. Multiple spray passes, each depositing a thin coating layer, are required to build up the desired coating thickness, which can be as thin as a few microns or as thick as desired, within reasonable limits. However, internal stresses are greater for thicker coatings, and the potential for cracking from differential thermal expansion increases with coating thickness.

The plasma spray process (e.g., Gordon England; 2003) builds on the flame spray method by replacing the oxy-fuel flame with a high-temperature electric arc similar to that used for electric arc welding. This allows for effective spraying of materials with higher melting temperatures (e.g., refractory metal, such as tungsten, and ceramics, such as zirconia) than is possible with the flame spray process. Inert carrier gases also significantly reduce the degree of oxidation of metallic coating materials. Deformation of the softened or molten spray particles upon impact produces better bonding, both to the substrate and between coating particles. The high impact velocity of the particles results in an overlaying edges or "imbricated" coating structure, with the potential also for a higher density coating than is possible with the flame spray process. The coating density is a function of the spray process parameters. (Fincke and Swank, 1992) Coating densities produced by plasma spraying can be greater than 90% of theoretical density, although significantly lower density coatings (as low as 50%) can also be produced via plasma spraying.

In a typical system, the plasma spray gun consists of a copper anode and tungsten cathode, both of which are water cooled. The inert plasma gas (argon, nitrogen, hydrogen, helium) flows around the cathode and through the anode which is shaped as a constricting nozzle (see Figure 3). The plasma is initiated by a high voltage discharge which causes localized ionization and a conductive path for a DC arc to form between the cathode and anode. The resistance heating from the arc causes the gas to reach extreme temperatures, dissociate, and ionize to form a plasma. The plasma exits the anode nozzle as a free or neutral plasma flame. Powder is fed into the plasma flame most commonly via an external powder port mounted near the anode nozzle exit. The powder is so rapidly heated and accelerated that spray distances can range from 25 to 150 mm.
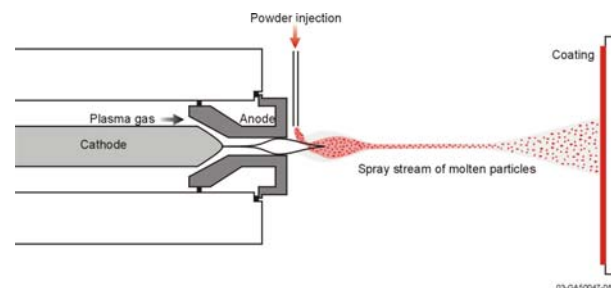
Figure 3. Representative setup for plasma spraying.

3

Copyright © 2004 by ASME

Considerations to Optimize Coating Performance

To optimize the performance of the plasma spray coating, several options are available, such as substrate surface preparation, plasma spray coating parameter optimization, and the inclusion of a "bond" coating between the substrate and the ceramic overlayer. INEEL investigated all three of these options. (Wright, 2000)

Cleaning and grit blasting are important for substrate preparation. This provides a more chemically and physically active surface needed for bonding. First, samples are cleaned to remove any surface grease that could affect the adhesion of the coating. Then, the surfaces are grit blasted to roughen the surface, which will in turn increase the coating bond strength.

The performance of the coating can be optimized by adjusting several parameters associated with the plasma spray coating process itself, including the plasma spray, powder feedstock material injection and processing variables. Plasma spray variables include the gun configuration, process gases, pressures, flow rates, voltage, amperage, and carrier gases. The powder feedstock variables include chemistry, morphology, particle size distribution, and method of manufacture. It is also possible to enhance some spray material properties by adding other materials. Material injection variables include powder feed rate, carrier gas flow, number of injectors, angle of injection, and location of injection. (Fincke, et al., 1997) Processing variables include the number of passes, spray distance, spray trajectory, traverse speed, tool fixturing and part cooling.

Inclusion of a "bond" coat layer between the substrate and its ceramic coating has been found to improve thermal barrier coating (TBC) performance. In some cases, bond coatings have been found to adhere better to the substrate, provide high temperature corrosion and oxidation protection for the substrate, create a rough surface for improved topcoat adhesion, and can reduce the residual stress that is a result of the coefficient of thermal expansion mismatch between the metallic substrate and the ceramic topcoat. Thermal spray materials like molybdenum and aluminium / metal composites are typically used as bond coatings.

Material Property Considerations

During the first year of this project, scoping materials evaluations identified candidate substrate and coating materials for the core catcher.

Stainless steel 304 and carbon steel SA533 are candidate base materials. Thermal and structural properties for these materials are similar (Rempe, et al., 1993). Although carbon steel is less expensive than stainless steel, the use of stainless steel avoids the need to add a corrosion-resistant undercoating on the core catcher.

Hence, stainless steel was used as the substrate material for these materials interaction tests.

Initially, cerium dioxide, magnesium oxide, and zirconium dioxide were identified as promising candidates for for the core catcher upper surface insulator coating. As indicated in Table 1, all three materials have relatively high melting points and low thermal conductivities (INEEL, 2002; Touloukian, 1967). The coating material must also be resistant to cracking (so that it can protect the base material). Although thermal-shock resistance cannot be measured quantitatively, a figure of merit proposed by Winkelmann and Schott (1984) was applied to estimate the relative resistance of various materials to thermal shock. Evidence supporting the use of this coefficient is limited. However, it does provide some measure of the material's shock resistance. Experimental evidence suggests that materials with lower values for a coefficient of thermal endurance are less resistant to thermal shock.

The potential for interactions between core catcher and relocated corium materials was also evaluated using phase diagram information (Levin, et al., 1985). Initial evaluations suggested that MgO exhibited superior performance. However, ZrO_2 powder is considerably less expensive than MgO. In addition, there is considerable more experience with applying yttria-stabilized ZrO_2 using plasma spray techniques. Hence, samples with coatings containing MgO and ZrO_2 were prepared and evaluated.

Table 1. Properties of candidate coating materials.

Material	Melting Temperature, K	Thermal Conductivity, W/m°C (@1273 K)	Coefficient of Thermal Endurance	Cost ($/kg)[a]
CeO_2	2610	1.7	0.01	$83
MgO	3070	7.5	0.02	$70
ZrO_2	2980	1.0	0.04	$42
$MgOZrO_2$[b]	2413	2.6	0.04	$70
$MgAl_2O_4$[c]	2273	5.4	0.05	$70

a. Except for the Sulzer Metco price for $MgOZrO_2$, prices based on information available in CERAC March 2003 catalogue for high purity mesh 325 powder (cost for preparing powder for spraying is not included).
b. Sulzer Metco 210NS-1 magnesium zirconate is 76 wt% ZrO_2 and 24 wt% MgO.
c. Saint-Gobain spinel magnesium aluminate is 77 wt% Al_2O_3 and 23 wt% MgO.

Initially, it was desired to apply high purity (99.99%) MgO coatings. However, several thermal spray vendors explored methods to apply this material without any success. Although several independent spray laboratories varied parameters associated with the powder, the gas type and flowrate, spray gun nozzle and type, the best coating that could be produced was extremely thin and friable (it could be removed with slight rubbing). These thermal spray organizations speculated that this material was not suitable for this plasma thermal

4   Copyright © 2004 by ASME

spraying because its vaporization temperature was relatively close to its melting temperature (MgO melts at 3070 K and vaporizes at 3530 K; whereas ZrO_2 melts at 2980 K and vaporizes at 5270 K). However, when the MgO material was combined with Al_2O_3, a much thicker coating could easily be obtained. Although thermal spray experience indicates that Al_2O_3 is very effective at providing protection against oxidation, the addition of Al_2O_3 affects the liquidus temperature of the coating (As shown in Figure 4, the addition of 30% Al_2O_3 lowers the liquidus from 3080 K to 2730 K).
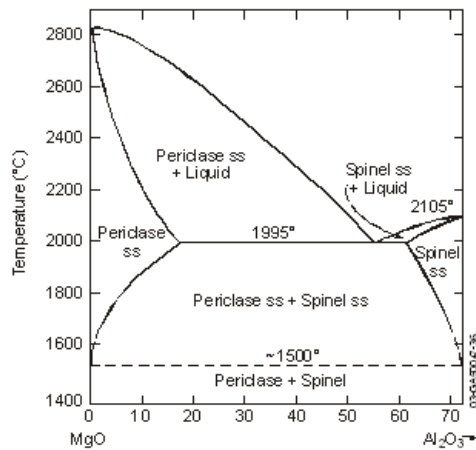
Figure 4. MgO and Al_2O_3 phase diagram in weight percent. (Levin, et al., 1985)

In addition, several MgO-containing compounds were investigated, such as magnesium zirconate and magnesium aluminate. Thermal spraying experience at INEEL has found that magnesium oxide coatings are easier to apply and perform better when the magnesium oxide is chemically combined with alumina and zirconia (Sulzer Metco, 2000; Saint-Gobain, 1998).

As discussed above, the use of bond coatings has been found to improve the performance of thermal spray coatings. INEEL investigated three bond coating materials: 100% nickel, a 95% nickel / 5% aluminum alloy, and Inconel 718. References (Touloukian, 1977a; Touloukian, 1977b; ASM; 1996) indicate that these materials have similar melting temperatures (1610-1730 K), but much higher thermal conductivities than proposed substrate materials. However, information in ASM suggests that the inclusion of aluminum in the bond coating could lead to reactions with iron and coating materials at relatively low temperatures.

The coefficient of thermal expansion is an important consideration in evaluating if the coatings and substrate are compatible. Figure 5 compares thermal expansion coefficients of candidate coating, base, and substrate materials (Touloukian, 1978; Rempe, 1993). Results in the figure indicate that magnesium oxide may be a good

choice for a coating material because its expansion and contraction are most closely aligned with the expansion and contraction of the proposed base materials. Curves in Figure 5 also suggest that the nickel bond coating material may reduce differences between expansion of proposed oxide coating and substrate materials.
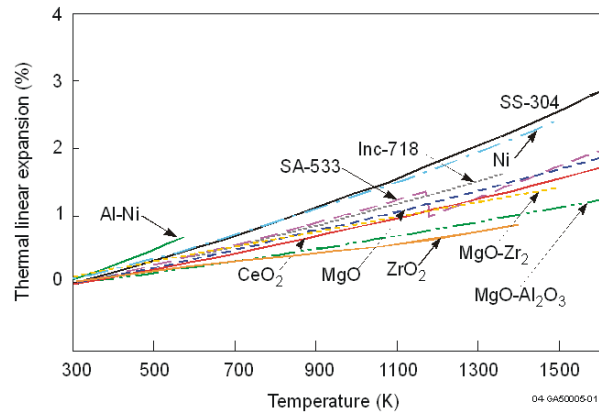
Figure 5. Insulator, bond, and base material thermal expansion coefficients.

Test Approach - Sample & Setup

As part of the investigation to select an appropriate core catcher coating, samples were prepared for conducting all of the tests listed in Table 2. As discussed above, several types of ceramic coatings were considered. Because ZrO_2 coatings are less expensive and widely used, initial investigations considered this ceramic material. Then, samples with coatings containing MgO were prepared with the bond coating/ coating thickness combinations deemed to yield the optimum performance.

Table 2. Coating parameter sensitivities

Parameter	Range
Coating Thickness	200, 500, and 1000 μm
Bond Coating	100-200 μm thick Ni, Ni-Al, or Inconel-718 bond coating or no bond coating.
Oxide Material	zirconium dioxide magnesium oxide[a] magnesium zirconate spinel magnesium aluminate
Thermal Spray Parameters[b]	Nominal case Fewer cracks / lower density More cracks / higher density

a. As noted above, Al_2O_3 powder was "mixed" with the magnesium oxide in order to obtain a thermal spray coating.

b. Varied range of thermal spray parameters, such as carrier gas composition, carrier gas flowrate, torch current, standoff distance, and traverse speed, to obtain desired coating properties.

5   Copyright © 2004 by ASME

Figure 6 contains photos of uncoated and coated samples. Samples were machined from 1 inch stainless steel (SS 304) rod. Each sample was approximately 2 inches long. Prior to the application of any coating, samples were grit blasted and degreased. As discussed above, this process enhances the adhesive strength of the TBC.
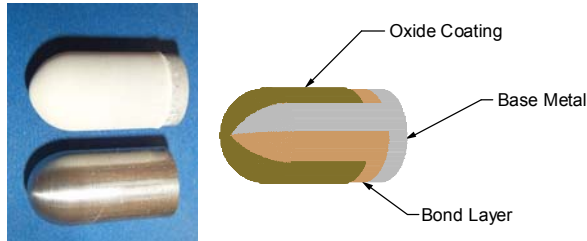
Figure 6. Samples with and without spray coating and diagram illustrating spray coating layers.

Figure 7 illustrates the configuration used to heat samples in a Carbolite tube furnace. This horizontal tube furnace is rated at 1700 ºC and can accept alumina working tubes up to 75 mm inside diameter and 600 mm long. During testing, the furnace temperature was set to 1400 ºC (this temperature is used because it is just below the stainless steel melting point). This temperature was checked (and found to be accurate) with a two-color optical pyrometer.
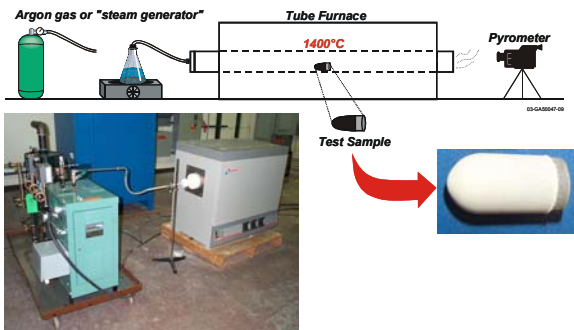
Figure 7. Setup for sample testing.

As shown in Figure 7, a steam or argon environment was obtained by flowing the vapor or gas through one end of the tube furnace for a period of 30 minutes prior to testing. At the end of the planned test period (a 5 minute "warm up" at the furnace entrance followed by a 10 minute heating period), the flow is stopped, and the specimen is slowly removed from the furnace. Samples were individually tested to avoid unwanted interactions between oxides.

Although this setup provides insights about coating performance, several differences exist between the test setup and the conditions to which a core catcher will be exposed to during a severe accident. Some of these differences include:

- Temperatures are below temperatures of molten materials that may relocate during a severe accident.
- Test samples have an uncoated end, which is used to hold the sample during thermal spraying, whereas the entire upper surface of the core catcher would be coated.
- The entire sample is subjected to high temperatures; whereas hot materials will only be near the core catcher upper surface.

In reviewing test results and assessing coating, the above differences were reviewed to determine if phenomena observed during the tests are relevant.

MATERIALS TEST RESULTS

Bond Coating Performance

The first material tests were run to evaluate the benefit of including a bond coating between the oxide and stainless steel sample. These tests used 500 µm ZrO_2 TBCs on top of 100-200 µm bond coatings. Duplicate samples were prepared so that one could be run in steam and one could be run in argon (However, samples with Inconel-718 bond coatings were tested near the end of this effort, and both run in steam). Observations from these tests are summarized below.

- *Cracking and oxidation was more pronounced in steam tests.* The endstates for samples with Nickel Aluminum bond coatings beneath a ZrO_2 coating (designated as NA-1 and NA-2) are shown in Figure 8. These endstates illustrate that degradation was more pronounced in samples run in steam.
- *Minimal materials interactions were observed.* The end states of samples suggest that minimal materials interactions occurred between the stainless steel, bond coatings, or zirconia coatings.
- *Additional oxidation, cracking, and spallation occurred during cooldown.* Additional sample oxidation, cracking, and spallation occurred during the cooldown period after the sample was removed from the furnace.
- *The nickel and nickel-aluminum bond coatings did not enhance "bonding".* As shown in Figure 9, the samples with a nickel bond coating (N-1) and a nickel-aluminum bond coating (NA-1) appeared to experience more thermal expansion and contraction than either the zirconia coating or stainless steel substrate.
- *The zirconia coating with the Inconel 718 bond coating and the zirconia coating without any bond coating provide the best protection.* As shown in Figure 9, the sample with the Inconel 718 (I-1) bond

6 Copyright © 2004 by ASME

coating appears to provide the best protection (although the sample without any bond coating (G-1) also appears to provide adequate protection to the substrate material).

NA-1; 500 μm in steam   NA-2; 500 μm in argon
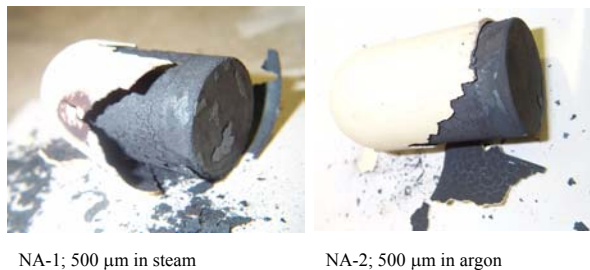
Figure 8. Endstates of samples with nickel-aluminum bond coatings.

(NA-1: 500 μm)   (N-1: 500 μm)

(G-1: 500 μm)   (I-1:500 μm)
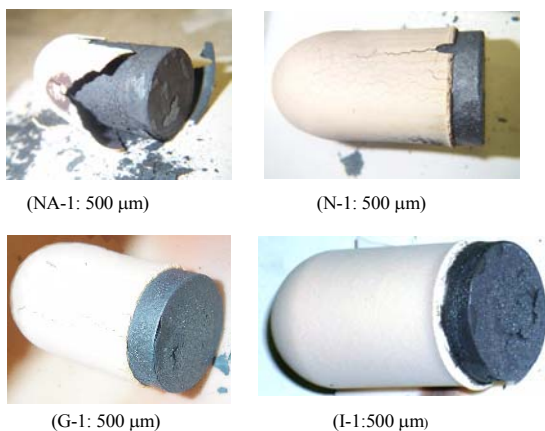
Figure 9. Endstates for samples tested in steam to investigate the impact of bond coatings.

Oxide Coating Thickness

Figure 10 compare endstates from selected samples to investigate the impact of coating thickness. Observations from these tests are summarized below.

- *Significantly more materials interactions and oxidation occurred in tests with steam.* Oxidation in tests with argon was similar to that observed in the initial tests. However, as shown in Figure 10, sample degradation was much more pronounced in steam tests for all three samples prepared without any bond coating (G-3, G-5, and G-7). As shown in Figure 11, several samples were prepared with 500 μm coatings similar to the G-1 sample and tested in steam (samples G-3, G-9, and G-10). Materials interactions were observed in all of these samples except the G-1 sample. Post-test exams and thermal spray parameter sensitivity tests did not provide any additional insights about the superior performance of the G-1 sample coating.

- *Coating thickness significantly affects the amount and type of degradation.* The endstates shown in Figure 10 suggest that thinner coatings allowed oxygen to penetrate the underlying steel and degrade the sample's outer surface. Thicker coated samples were able to retain fairly intact coatings (although cracking and flaking occurred during cooldown). In steam tests, the thinner coating on the G-5 sample became perforated with large holes. Deposits were also observed on the outer surface of samples with thicker coatings that were tested in steam. However, these deposits appeared to be due to material that flowed from uncoated regions of the samples.

- *The coating should be at least 500 μm thick.* Figure 10 suggests that coatings thinner than 500 μm are not able to provide adequate sample protection. In the case of the steam tests, the perforated coating endstate of the G-5 sample demonstrates that a 200 μm coating is not sufficient to protect the underlying substrate material. Although iron oxide deposits were observed on samples with thicker coatings, the substrate material appears fairly intact.

G-5; 220 μm in steam

G-3; 500 μm in steam

G-7; 1000 μm in steam
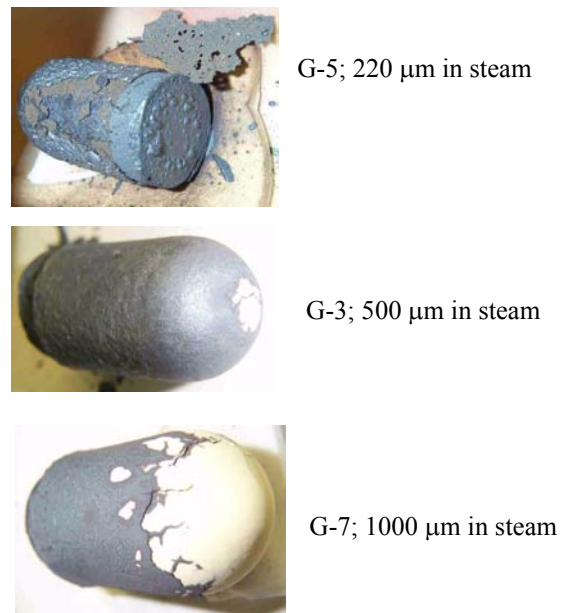
Figure 10. Selected endstates of samples tested to investigate the impact of coating thickness.

Oxide Material

A third series of materials tests was conducted on samples with coatings containing magnesium oxide. Table 3 identifies the composition of coatings in each sample tested. Note that the MgO and Al_2O_3 in powders for samples M-1 through M-10 were simply mixed. Samples designated with MZ and MA have been prepared with powders that have the MgO chemically combined with the ZrO_2 or Al_2O_3 to form a compound.

7   Copyright © 2004 by ASME

(G-1: 500 μm)

(G-3: 500 μm)

(G-9: 500 μm)

(G-10: 500 μm)

Figure 11. End states of 500 μm ZrO_2-coated samples tested in steam.

In addition, these powders are specially prepared to optimize coating performance (Sulzer Metco, 2000; Saint-Gobain, 1998). For example, the MZ sample was sprayed with Metco 210NS-1 powder, a spherical free-flowing prestabilized magnesium zirconate powder.

Table 3. Magnesium oxide containing powders investigated.

Sample Designation	Coating Powder Composition
M-1 → M-8	Magnesium Oxide (70 wt%)-Aluminum Oxide (30 wt%) - mixed
M-9 → M-10	Magnesium Oxide (88 wt%)-Aluminum Oxide (12 wt%) - mixed
MZ-1 → MZ-2	Magnesium Oxide (24 wt%)-Zirconium Dioxide (76 wt%)
MA-1 → MA-2	Spinel Magnesium Oxide (23 wt%)- Aluminum Oxide (77 wt%)

Figure 12 compare endstates from various tests. Observations from these tests are summarized below.

- *No materials interactions were observed.* The endstates shown in Figure 12 do not suggest that any materials interactions occurred between these coatings and the underlying substrate material.
- *Cracking occurred with MgO-containing coatings that were 1000 μm thick.* These cracks were observed when these samples were first removed from the furnace and increased during cooling.
- *Coating performance degraded with samples sprayed with mixed powders initially containing higher MgO concentrations.* The endstate of the M-10 sample sprayed with powder initially consisting

(M-7; 500 μm) in steam

(M-10; 500 μm) in steam

(MZ-1; 500 μm) in steam

(MA-1; 500 μm) in steam
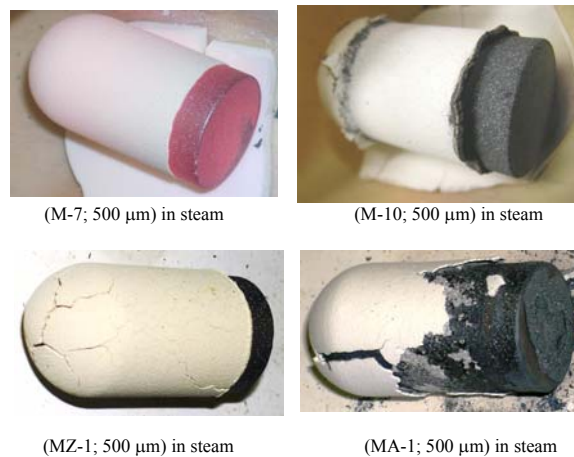
Figure 12. Endstates of samples with MgO-containing coatings tested in steam.

of 88 wt% MgO /12 wt% Al_2O_3 is shown in Figure 12. Note that this sample, which was tested in steam, exhibited significant cracking on the curved surface. Furthermore, the lower edge of the coating detached from the substrate material.

- *Coatings with mixed MgO-Al_2O_3 powders do not provide adequate protection.* Figure 13 shows a macrophotograph of a sample sprayed with a 70 wt% MgO/ 30 wt% Al_2O_3 powder. As shown in this photograph, the coating is relatively dense and adheres well to the substrate material. However, EDS examinations revealed that this coating contained less than 0.5 wt% Mg (rather than the expected 41 wt% Mg for the initial powder composition). Hence, the coatings for samples M-1 through M-10 were of much higher concentrations of Al_2O_3 due to MgO vaporization during thermal spraying. Such high concentrations of Al_2O_3 yields melting temperatures of less than 2400 K (see Figure 4). Note that MgO vaporization did not occur with either the magnesium zirconate or magnesium aluminate compounds investigated.
- *The magnesium zirconate coating protected the substrate with minimal cracking and no materials interactions.* The endstate for this sample shown in Figure 12 shows that the coating experienced minimal cracking or spallation during cooldown (much less than observed with the magnesium aluminate coating). In addition, no materials interactions occurred between this coating and the underlying substrate material.

8

Copyright © 2004 by ASME
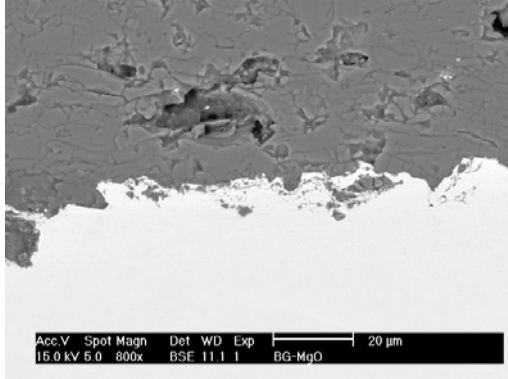
Figure 13. Magnification of representative coating for M-1 through M-8 tests (800X)

Thermal Spray Parameter Sensitivities

As noted above, the plasma spray coating process has many variables that can affect the characteristics of the coating. Coating porosity/density, adhesion, and crack structure are a function of the sprayed particle temperature, velocity and application parameters. INEEL's extensive diagnostic capability allows an understanding of how torch operating variables are related to the plasma gas flow field and how the sprayed particle condition prior to it being deposited on the substrate is related to the characteristics of the coating. By understanding these relationships, it is possible to efficiently develop spray parameters that result in coatings and materials with the desired characteristics. At the same time, a clear picture is developed of which parameters have narrow operating windows that must be tightly controlled for consistent production of high quality coatings and materials.

Table 4 lists the nominal spray process parameters used to create the coatings tested in this study. Nominal torch configuration and settings are also listed in Table 4. Sensitivity tests were conducted to investigate the process variables of torch power, total gas flow, argon to helium ratio in the gas mix, spray distance and individual spray layer thickness. Each of these parameters was varied from the nominal conditions listed in Table 4. For each of these variations, the sprayed particle velocity and temperature were measured using Laser Doppler Velocimetry and a two-color pyrometry technique respectively. (Fincke, et al., 2001; Swank, et al., 1995) The measurements indicate that the average particle velocity varies about 20 m/s and the average particle temperature varies approximately 200 °C.

Table 4. Nominal spray process parameters.

Parameter	Value
Substrate	304 SS grit blasted with 30 micron Alundum
Coating Material	Saint Gobain 204F Zirconia
Torch	Praxair SG-100
Anode/Cathode/Gas ring	Genie 730/720/112
Standoff Distance	100 mm
Torch Current	800 Amps
Torch Gases:	
Argon flow rate	30 slm (standard liters per minute)
Helium flow rate	10 slm
Argon carrier gas flow rate	3 slm
Powder feeder	Praxair 1270 Roto feed
Feeder Rotational Velocity	2 rpm
Traverse Speed	100 mm/sec

For these sensitivity tests, zirconia coatings were sprayed on half-sections of 2 inch long Inconel 718 1/4-inch thick tubing. This substrate material was selected to avoid interactions between zirconia and iron oxide. After heating half-sections at 1400 °C for 10 minutes in steam, samples were cooled and coatings were examined macroscopically. Measured variations in particle condition were found to be sufficient to cause differences in coating adhesion, density and cracking. For the nominal conditions, ZN-1, both vertical and horizontal cracking is evident. The coating appears to be lifted from the substrate. However, there is evidence that the coating did adhere to the grit blasted surface and that the bond failed within the coating rather than at the substrate coating interface.

A representative coating produced at a condition of relatively high particle velocity and temperature was designated as the ZM-3 parameters. Significantly more cracks appear, both horizontally and vertically, with extensive separation of the coating from the substrate. These characteristics are typical of higher residual stress that results from higher temperature and velocity deposition. A coating produced with lower spayed particle temperature and velocity relative to the one fabricated at the nominal conditions is designated as the ZC-2 parameters. Typical of other relatively low particle velocity and temperature coatings, ZC-2 shows fewer cracks, better adhesion and slightly lower density.

In an attempt to determine the effect of coating cracks and coating density on coating performance, test samples were prepared at the nominal condition ZN-1, at the ZM-3 condition that produced slightly higher density with significantly more cracks and at the ZC-2 condition that resulted in lower density and fewer cracks. As in other tests, these samples were heated at 1400 °C for 10 minutes in a steam environment. As shown in Figure 14,

9   Copyright © 2004 by ASME

none of these sample coatings precluded iron oxide formation. In all three cases, oxygen was able to penetrate through the coating to oxidize the underlying substrate material.

ZN-1; 500 µm in steam

ZM-3; 500 µm in steam

ZC-2; 500 µm in steam
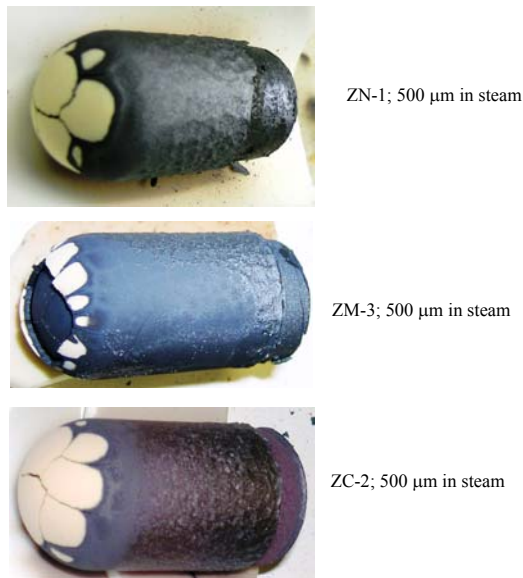
Figure 14. Endstate of samples developed for thermal spray parameter sensitivity tests, tested in steam.

SUMMARY

A series of materials interaction tests have been completed to provide insights about the coatings that should be used for an internal core catcher. Results from these tests suggest that two coatings can provide adequate protection to a stainless steel core catcher:

- A 500 µm thick zirconium dioxide coating over a 100-200 µm Inconel 718 bond coating.
- A 500 µm thick magnesium zirconate coating.

Commercial plasma sprayed thermal barrier coatings are typically fabricated with a bond coat layer to increase bond strength and reduce coating residual stress. (Swank, 2000) Thus, using a corrosion resistant bond coat of Inconel 718 is expected to perform better at the high temperature, oxidizing conditions expected during a severe accident. Hence, initial prototypic tests will use this coating. Activities are underway at INEEL to prepare for these high temperature prototypic tests.

ACKNOWLEDGMENTS

REFERENCES

ASM, 1996, *Binary Alloy Phase Diagrams*, Second Edition, Plus Updates, Version 1.0.

Fincke, J.R, W.D. Swank, and D.C. Haggard, 1997, "The influence of Injector geometry and Carrier Gas flow Rate on Spray Pattern and Particle Temperature," *Thermal Spray: A United Forum for Scientific and Technological Advances (UTSC'97)* ed. C. C. Berndt, ASM International, pp.335-342, Indianapolis, IN.

Fincke, J.R. and W.D. Swank, 1992, "Air-Plasma Spraying of Zirconia: Spray Characteristics, Deposition Efficiency and Porosity Control by Standoff Distance," *1992 International Thermal Spray Conference, Orlando,* May 1992.

Fincke, J.R., et al., 2001,"Diagnostics and Control in the Thermal Spray Process", *Surface and Coatings Technology*, 2001, 146-147, pp 537-543

Hwang, I. S., and K. Y. Suh, 2001, "Gap Structure for Nuclear Reactor Vessel," United States Patent US 6, 195, 405 B1, Registered February 2001.

INEEL, 2002, SCDAP/RELAP5-3D[©] Development Team, *SCDAP/RELAP5-3D[©] Code Manuals*, INEEL/ EXT-02/00589, Idaho National Engineering and Environmental Laboratory, May 20, 2002.

Levin, E.M., et al., 1985, "Phase Diagrams for Ceramists, Volume I," *The American Ceramic Society, Inc.,* Columbus, Ohio, Fifth Printing.

Gordon England, 2003, *Plasma Spray Process*, website, www.gordonengland.co.uk; accessed March 16, 2003.

Rempe, J. L, et al., 1993, *Light Water Reactor Lower Head Failure Analysis,* NUREG/CR-5642, October 1993.

Rempe, J. L., et al., 2002, *In-Vessel Retention Strategy for High Power Reactors,* 2002 Annual Report, INEEL/ EXT-02-01291, October 2002.

Saint-Gobain, 1998, *MSDS for Spinel Magensium Aluminate*, dated September 21, 1998.

Swank, W. D., J.R. Fincke, and D. C. Haggard, 1995, "A Particle Temperature Sensor for Monitoring and Control of the Plasma Spray Process," *Advances in Thermal Spray Science and Technology (NTSC'95),* eds. C. Berndt and S. Sampath, ASM International, 111-116, Houston, TX.

Swank, W. D. , et al., 2000, "Residual Stress Determination from a Laser-Based Curvature Measurement," *Thermal Spray; Surface Engineering via Applied Research,* C. C. Berndt, ed., ASM International, Materials Park, OH, pp. 363-369.

10   Copyright © 2004 by ASME

Sulzer Metco, 2000, *Metco 210NS-1 Magnesuim Zirconate Powder*, Technical Bulletin #10-280, October 2000.

Touloukian, Y.S., Editor, 1967, *Thermophysical Properties of High Temperature Solid Materials, Volume 4: Oxides and their Solutions and Mixtures, Part I: Simple Oxygen Compounds and Their Mixtures*, MacMillan Company, New York.

Touloukian, Y. S., et al., 1977a, *Thermal Expansion, Metallic Elements and Alloys, Thermophysical Properties of Matter*, Volume 12, Plenum Publishing Company, New York, 2nd Printing.

Touloukian, Y. S., et al., 1977b, *Thermal Conductivity, Metallic Elements and Alloys, Thermophysical Properties of Matter,* Volume 1, Plenum Publishing Company, New York, 2nd Printing.

Touloukian, Y. S, et al., 1978, *Thermophysical Properties of Matter, Volume 12, Thermal Expansion Metallic Elements and Alloys*, IFI Plenum Publishing, New York.

Winkelmann, A. A and O. Schott, 1894,"Dependence of Thermal Resistance Coefficients of Glasses on their Chemical Composition," *Ann. Physik Chem.* 51, 730-745.

Wright, R.N and W. D. Swank, 2000, "Microstructure Effects on Stainless Steel Substrates from Deposition of Plasma Spray Coatings," *Thermal Spray; Surface Engineering via Applied Research,* C. C. Berndt, ed., ASM International, Materials Park, OH, pp. 9-14.

11